



Contents lists available at ScienceDirect

Arabian Journal of Chemistry

journal homepage: www.ksu.edu.sa

New sesqueneolignan glycoside isomers from the aerial parts of *Leonurus japonicus* and their absolute configurations

Lan Bu^{a,c,1}, Qin-Mei Zhou^{a,d,1}, Cheng Peng^a, Hong-Zhen Shu^a, Fei Zhou^a, Guang-Xu Wu^a, Fei Liu^a, Hui Tian^{b,*}, Liang Xiong^{a,*}

^a State Key Laboratory of Southwestern Chinese Medicine Resources, School of Pharmacy, Chengdu University of Traditional Chinese Medicine, Chengdu 611137, China

^b Key Laboratory for Quality Control and Evaluation of Traditional Chinese Medicine of Mianyang City, Mianyang Normal University, Mianyang 621000, China

^c State Key Laboratory of Bioactive Substance and Function of Natural Medicines, Institute of Materia Medica, Chinese Academy of Medical Sciences and Peking Union Medical College, Beijing 100050, China

^d Innovative Institute of Chinese Medicine and Pharmacy, Chengdu University of Traditional Chinese Medicine, Chengdu 611137, China

ARTICLE INFO

Keywords:

Leonurus japonicus
Sesqueneolignan glycosides
Absolute configuration
Anti-inflammation

ABSTRACT

The acid water-soluble fraction of the 95% EtOH extract of *Leonurus japonicus* exhibited significant anti-inflammatory activity by suppressing the p-ERK/ERK ratio and iNOS expression. A further phytochemical investigation of this acid water-soluble fraction led to the isolation of three previously undescribed sesqueneolignan glycosides, leolignosides A–C (1–3), and their planar structures were elucidated using HR-ESI-MS and 1D and 2D NMR. To determine the complicated absolute configuration of sesqueneolignan glycosides, coupling constants, NOESY data, empirical rules, enzymatic hydrolysis, and ECD data were comprehensively used. These isolated compounds were also screened for anti-inflammatory activity. Encouragingly, leolignosides A–C all suppressed LPS-induced NO overproduction in RAW 264.7 macrophages. The aglycone (3a) of leolignoside C was chosen for further investigation for its activity and the available amount. Similar to the acid water-soluble fraction, compound 3a inhibited NO overproduction and decreased the p-ERK/ERK and p-NF-κB/NF-κB ratios, indicating that 3a may exert anti-inflammatory effects through the ERK/NF-κB signaling pathway.

1. Introduction

The aerial parts of *Leonurus japonicus* Houtt. (Chinese motherwort), known as an “excellent medicine for obstetrical and gynecological diseases”, have been used as an important medicine for treating postpartum hemorrhage and regulating menstruation in China for >1800 years (Miao et al., 2019). Given its role in clinical practice, our previous studies focusing on its traditional efficacy achieved several results. For example, alkaloids are the main material basis of motherwort for uterine contraction and hemostasis (Liu et al., 2018). Meanwhile, alkaloids also play a key role in treating postpartum uterine subinvolution due to their pro-angiogenic effects (Zhou et al., 2020). Motherwort terpenoids and steroids have significant vasodilatory and anti-platelet aggregation activities (Peng et al., 2013; Ye et al., 2014; Xiong et al., 2015a; Xiong et al., 2015b; Zhou et al., 2015; Zhou et al., 2019). In addition, flavonoids (Liu et al., 2018) and other compounds (Zhou et al., 2013) were also studied. Although some lignans have been reported from the fruits

of *L. japonicus* (Tian et al., 2021; Peng et al., 2021), a survey of the literature revealed that no more than 20 lignans have been reported from *L. japonicus*, and these do not include sesqueneolignans.

Chirality is an essential attribute of most natural products and is closely related to their pharmacological activities. Multiple chiral centers are usually present in lignans, which makes it difficult to determine their absolute configurations. This is especially true for sesqueneolignans containing multiple isolated chiral centers, as well as rotatable branched chains. Although great efforts have been made to determine the configurations of lignans, many studies only reported planar structures or relative configurations of lignans, especially sesqueneolignans (Macías et al., 2004; Yin et al., 2016; Zhuang et al., 2018; Zhao et al., 2020), reflecting the notion that the determination of the absolute configurations of sesqueneolignans is difficult. As part of an effort focused on bioactive secondary metabolites from motherwort, three new sesqueneolignan glycosides (1–3) with the same planar structure and different absolute configurations were discovered (Fig. 1). To determine their

* Corresponding authors.

E-mail addresses: tianhui1009@126.com (H. Tian), xiling@cducm.edu.cn (L. Xiong).

¹ Both authors contributed equally to this work.

<https://doi.org/10.1016/j.arabjc.2024.105932>

Received 25 February 2024; Accepted 22 July 2024

Available online 26 July 2024

1878-5352/© 2024 The Author(s). Published by Elsevier B.V. on behalf of King Saud University. This is an open access article under the CC BY-NC-ND license (<http://creativecommons.org/licenses/by-nc-nd/4.0/>).

absolute configurations, coupling constants, NOESY data analysis, enzymatic hydrolysis, empirical rules, and electronic circular dichroism (ECD) calculations were used in this study.

In addition, inspired by the traditional efficacy of motherwort and its clinical application in inflammatory gynecological diseases, the anti-inflammatory activities of the extract and the sesquieolignans were evaluated. NF- κ B is a key regulator of inflammatory responses and commonly forms a complex with I κ B in the cytoplasm. When the cells are stimulated by inducers, I κ B is expeditiously phosphorylated, ubiquitinated, and degraded. Then, NF- κ B translocates to the nucleus and binds to cognate DNA binding sites, triggering the transcription of many genes, including cytokines, chemokines, and enzymes. Inducible nitric-oxide synthase (iNOS) plays an important role in NO synthesis and secretion, which initiate and sustain the inflammatory process. What's more, a lot of natural products could exert anti-inflammatory activity through the NF- κ B/iNOS pathway (Li et al., 2019; Sun et al., 2017; Zuo et al., 2024). Therefore, the expressions of related proteins were also investigated in this study.

2. Materials and methods

2.1. General experimental procedures

A Rudolph Autopol-I automatic polarimeter (Rudolph Research Analytical, USA) was applied to measure optical rotations. IR spectra were recorded using a Cary 600 FT-IR microscope (Agilent Technologies Inc., CA, USA). ECD spectra were detected on a Chirascan-plus Circular Dichroism spectrometer (Applied Photophysics Ltd., Leatherhead, England). A Bruker TIMS-TOF-MS instrument (Bruker Corporation, Billerica, MA, USA) was applied to acquire HR-ESI-MS data. NMR data were obtained using a Bruker-AVIIIHD-600 spectrometer (Bruker Corporation, Billerica, MA, USA) with the solvent peaks as the references. Column chromatography was performed using silica gel (200–300 mesh, Yantai Institute of Chemical Technology, Yantai, China), MCI gel CHP 20P (40–60 μ m, Mitsubishi Chemical, Co., Japan), and Toyopearl HW-40F (TOSOH, Tokyo, Japan). TLC was performed using GF₂₅₄ silica gel plates (Anhui Liangchen Silicon Source Material Co. Ltd., Anhui, China). HPLC separation was carried out on an Agilent 1100 instrument equipped with a Zorbax SB-C₁₈ (9.4 \times 250 mm², 5 μ m). The hydrolysis reactions were carried out with snailase (Beijing BioDee Biotechnology Co., Ltd., Beijing, China). Curcumin was used as a positive control and purchased from Sichuan Weikeyi Biological Technology Co., Ltd. (Sichuan, China). NO levels were detected by nitric oxide assay kit from Beyotime Institute of Biotechnology (Shanghai, China). Rabbit anti-phospho-ERK1/2 (Thr202/Tyr204) and anti-ERK1/2 antibodies were purchased from Cell Signaling Technology (CST; Danvers, Massachusetts, US). Rabbit anti-phospho-NF- κ B (Ser536) and anti-NF- κ B antibodies were obtained from Chengdu Zen Bioscience Co., Ltd. (Chengdu, China). Rabbit anti-iNOS was bought from Beyotime Institute of

Biotechnology (Shanghai, China). Rabbit anti- β -actin antibody was gained from GeneTex Inc. (Irvine, California, USA). Peroxidase-conjugated AffiniPure goat anti-rabbit immunoglobulin G (IgG; [H+L]) was purchased from ZSGB-BIO Commerce Store (Beijing, China). Shanghai EpiZyme Biotechnology Co., Ltd. (Shanghai, China) supplied Omni-ECL TMFemtoLight chemiluminescence Kit.

2.2. Plant material

The aerial parts of *L. japonicus* were purchased from Sichuan Neautus Traditional Chinese Medicine Co., Ltd. in 2019 and identified by Prof. Jihai Gao at Chengdu University of Traditional Chinese Medicine. A voucher specimen (LJ-20190517) has been deposited at the school of pharmacy, Chengdu university of Traditional Chinese Medicine, China.

2.3. Extraction and isolation

The aerial parts of *L. japonicus* (100 kg) were refluxed three times with 95 % EtOH (3 h each time) to afford an EtOH extract, which was evaporated to give a residue (5.5 kg). The residue was suspended in water containing 1 % hydrochloric acid and partitioned with EtOAc. The acid water-soluble fraction (AWSF, 660 g) was subjected to a silica gel column using a gradient elution of ethyl acetate–methanol–ammonia (100:7:5–0:7:5) to afford 11 fractions (F₁–F₁₁). Eluting with a step gradient of 10–100 % MeOH in H₂O, F₅ was separated using flash chromatography over MCI gel to obtain six subfractions (F_{5.1}–F_{5.6}). F_{5.5} was fractionated via silica gel column chromatography over ethyl acetate–methanol–ammonia (100:5:5–0:5:5) to afford nine subfractions F_{5.5.1}–F_{5.5.9}. F_{5.5.4} was further purified using Toyopearl HW-40F column chromatography (50 % MeOH in H₂O), followed by reserved-phase semi-preparative HPLC (50 % MeOH in H₂O) to afford **1** (2.3 mg, t_{\min} = 102.4 min), **2** (1.3 mg, t_{\min} = 90.2 min), and **3** (1.9 mg, t_{\min} = 112.8 min).

Leolignoside A (**1**): white powder; $[\alpha]_D^{20}$ –4.8 (c 0.04, MeOH); UV (MeCN) λ_{\max} (log ϵ) 193 (4.4), 281 (3.0) nm; IR (ATR) ν_{\max} 3296, 2938, 2856, 1634, 1567, 1514, 1463, 1025, 771, 722 cm⁻¹; (+)-HR-ESI-MS m/z 797.2995 [M+Na]⁺ (calcd. for C₃₉H₅₀O₁₆Na, 797.2997); ¹H (CDCl₃, 600 MHz) and ¹³C NMR (CDCl₃, 150 MHz) data, see Table 1.

Leolignoside B (**2**): white powder; $[\alpha]_D^{20}$ –9.5 (c 0.04, MeOH); UV (MeCN) λ_{\max} (log ϵ) 202 (3.9), 280 (2.7) nm; IR (ATR) ν_{\max} 3355, 2925, 2854, 1666, 1595, 1517, 1457, 1075, 820, 742, cm⁻¹; (+)-HR-ESI-MS m/z 797.2995 [M+Na]⁺ (calcd. for C₃₉H₅₀O₁₆Na, 797.2997); ¹H (CDCl₃, 600 MHz) and ¹³C NMR (CDCl₃, 150 MHz) data, see Table 1.

Leolignoside C (**3**): white powder; $[\alpha]_D^{20}$ –4.8 (c 0.04, MeOH); UV (MeCN) λ_{\max} (log ϵ) 199 (4.3), 281 (3.0) nm; IR (ATR) ν_{\max} 3297, 2919, 2852, 1637, 1557, 1516, 1461, 1074, 763, 720 cm⁻¹; (+)-HR-ESI-MS m/z 797.2995 [M+Na]⁺ (calcd. for C₃₉H₅₀O₁₆Na, 797.2997); ¹H (CDCl₃, 600 MHz) and ¹³C NMR (CDCl₃, 150 MHz) data, see Table 1.

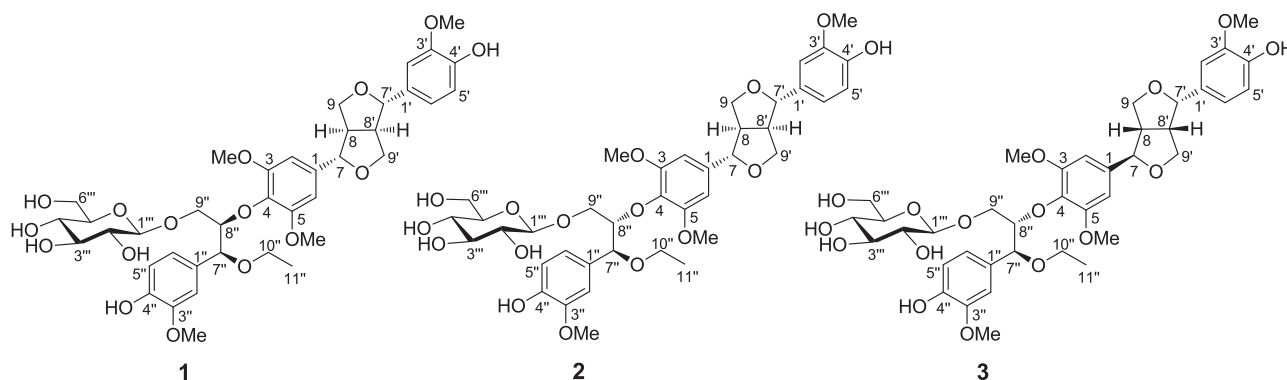


Fig. 1. Structures of sesquieolignagan glycosides 1–3.

Table 1¹H (600 MHz) and ¹³C NMR (150 MHz) data of compounds 1–3 (CDCl₃, δ in ppm, J in Hz).

No.	1		2		3	
	δ _H	δ _C	δ _H	δ _C	δ _H	δ _C
1	–	137.1	–	136.9	–	137.0
2	6.56 br.s	103.4	6.48 br.s	103.5	6.51 br.s	103.7
3	–	153.2	–	153.2	–	153.2
4	–	135.5	–	135.3	–	135.4
5	–	153.2	–	153.2	–	153.2
6	6.56 br.s	103.4	6.48 br.s	103.5	6.51 br.s	103.7
7	4.71 d (5.4)	86.1	4.68 d (5.4)	85.9	4.38 d (7.2)	87.8
8	3.06 m	54.6	3.02 m	54.6	2.85 m	54.8
9	4.25 dd (9.6, 7.2)	71.7	4.26 ^a	71.7	4.12 br. d (9.6)	71.1
	3.90 ^a		3.88 ^a		3.85 ^a	
1'	–	132.9	–	132.9	–	130.4
2'	6.90 d (1.8)	108.7	6.89 d (1.8)	108.7	6.94 d (1.8)	108.4
3'	–	146.9	–	146.9	–	146.6
4'	–	145.4	–	145.4	–	144.8
5'	6.90 d (8.4)	114.4	6.90 d (8.4)	114.4	6.89 d (8.4)	114.4
6'	6.82 dd (8.4, 1.8)	119.1	6.82 dd (8.4, 1.8)	119.1	6.78 dd (8.4, 1.8)	118.5
7'	4.76 d (4.8)	85.9	4.74 d (5.4)	85.9	4.86 d (5.4)	82.2
8'	3.12 m	54.2	3.09 m	54.1	3.32 m	50.2
9'	4.29 dd (9.0, 7.2)	72.2	4.26 ^a	72.1	3.83 ^a	70.0
	3.90 ^a		3.88 ^a		3.31 ^a	
1''	–	131.0	–	131.4	–	131.5
2''	6.76 d (1.8)	109.2	6.87 d (1.8)	109.8	6.88 d (1.2)	109.9
3''	–	146.6	–	146.4	–	146.4
4''	–	145.1	–	145.2	–	145.2
5''	6.81 d (8.4)	114.2	6.81 ^a	113.8	6.82 d (8.4)	113.8
6''	6.66 dd (8.4, 1.8)	120.2	6.80 ^a	121.0	6.81 dd (8.4, 1.2)	120.9
7''	4.53 d (3.6)	81.2	4.59 d (6.6)	80.7	4.60 d (6.0)	80.8
8''	4.36 ddd (7.8, 3.6, 1.8)	85.7	4.44 ddd (6.6, 3.6, 3.0)	83.3	4.42 ddd (6.0, 3.6, 3.0)	83.4
9''	4.19 dd (11.4, 1.8)	69.5	4.24 ^a	68.4	4.24 dd (11.4, 3.6)	68.3
	4.06 dd (11.4, 7.8)		3.85 ^a		3.85 ^a	
10''	3.45 q (7.2)	65.3	3.43 q (7.2)	65.0	3.44 q (7.2)	65.0
11''	1.25 t (7.2)	15.6	1.19 t (7.2)	15.4	1.19 t (7.2)	15.4
1'''	4.43 d (7.8)	104.1	4.36 d (7.8)	103.1	4.35 d (7.8)	103.0
2'''	3.24 dd (8.4, 7.8)	74.0	3.35 t (8.4)	73.9	3.34 ^a	73.8
3'''	3.50 dd (9.0, 8.4)	76.6	3.52 t (9.0)	76.8	3.53 t (9.0)	76.8
4'''	3.52 dd (9.0, 7.2)	70.5	3.56 t (9.0)	70.8	3.56 t (9.0)	70.8
5'''	3.36 m	75.3	3.33 m	75.4	3.34 ^a	75.4
6'''	3.86 ^a 3.77 dd (12.0, 4.8)	62.6	3.87 ^a	62.8	3.88 dd (12.0, 3.6)	62.8
			3.78 dd (12.0, 5.4)		3.78 dd (12.0, 4.8)	
OMe-3, 5	3.83 s	56.4	3.75 s	56.5	3.76 s	56.5
OMe-3'	3.91 s	56.1	3.91 s	56.1	3.92 s	56.1
OMe-3''	3.84 s	56.1	3.84 s	56.0	3.86 s	56.1
OH-4'	5.62 s	–	–	–	5.58 s	–
OH-4''	5.56 s	–	–	–	5.56 s	–

^a The ¹H NMR signal was overlapped.

2.4. Enzymatic hydrolysis

Compounds **1** (1.9 mg), **2** (1.0 mg), and **3** (1.5 mg) in H₂O (4 mL) were hydrolyzed with snailase (15 mg) at 37 °C for 48 h, respectively. After that, EtOAc was applied to extract aglycones three times (3 × 16 mL). Then, the aglycones **1a** (1.1 mg), **2a** (0.6 mg), and **3a** (0.8 mg) were purified using HPLC (50 % MeCN in H₂O), and their structures were determined using ¹H NMR (Table 2) and HR-ESI-MS. Compound **1a**:

Table 2¹H NMR (600 MHz) data of compounds **1a–3a** (CDCl₃, δ in ppm, J in Hz).

No.	1a	2a	3a
1	–	–	–
2	6.51 br.s	6.51 br.s	6.53 br.s
3	–	–	–
4	–	–	–
5	–	–	–
6	6.51 br.s	6.51 br.s	6.53 br.s
7	4.70 d (5.4)	4.70 ^a	4.39 d (7.2)
8	3.04 m	3.04 m	2.85 m
9	4.24 dd (9.0, 7.2)	4.25 dd (9.0, 7.8)	4.12 br.d (9.6)
	3.87 ^a	3.90 ^a	3.85 dd (9.6, 6.0)
1'	–	–	–
2'	6.94 d (1.8)	6.96 br.s	6.96 br.s
3'	–	–	–
4'	–	–	–
5'	6.86–6.92 ^a	6.94 d (8.4)	6.89 d (7.8)
6'	6.86–6.92 ^a	6.89 ^a	6.87 ^a
7'	4.73 d (5.4)	4.73 d (4.8)	4.85 d (5.4)
8'	3.09 m	3.08 m	3.31 m
9'	4.25 dd (9.0, 7.2)	4.24 dd (9.0, 7.2)	3.83 m
	3.89 ^a	3.90 ^a	3.31 m
1''	–	–	–
2''	6.86–6.92 ^a	6.88 br.s	6.88 br.s
3''	–	–	–
4''	–	–	–
5''	6.86–6.92 ^a	6.88 ^a	6.88 ^a
6''	6.81 dd (8.4, 1.8)	6.81 br.d (7.8)	6.78 br.d (7.8)
7''	4.69 d (3.6)	4.70 d (6.0)	4.71 d (6.6)
8''	4.08 m	4.08 m	4.08 m
9''	3.96 dd (12.0, 3.0)	3.95 m	3.97 m
	3.63 dd (12.0, 3.0)	3.70 dd (11.4, 3.0)	3.70 m
10''	3.48 q (7.2)	3.48 q (7.2)	3.48 q (7.2)
11''	1.21 t (7.2)	1.21 t (7.2)	1.21 t (7.2)
OMe-3, 5	3.74 s	3.74 s	3.74 s
OMe-3'	3.90 s	3.90 s	3.92 s
OMe-3''	3.89 s	3.89 s	3.90 s
OH-4'	5.61 s	5.60 s	5.58 s
OH-4''	5.57 s	5.56 s	5.56 s

^a The ¹H NMR signal was overlapped.

[α]_D²⁰ –16.0 (c 0.03, MeOH); CD (MeCN) 209 (Δε + 4.50), 239 (Δε + 0.41), 279 (Δε + 0.41) nm; (+)-HR-ESI-MS *m/z* 635.2461 [M+Na]⁺ (calcd. for C₃₃H₄₀O₁₁Na, 635.2468). **2a**: [α]_D²⁰ –3.6 (c 0.03, MeOH); CD (MeCN) 217 (Δε + 0.14), 233 (Δε – 0.48), 282 (Δε + 0.10) nm; (+)-HR-ESI-MS *m/z* 635.2463 [M+Na]⁺ (calcd. for C₃₃H₄₀O₁₁Na, 635.2468). **3a**: [α]_D²⁰ +11.5 (c 0.03, MeOH); CD (MeCN) 216 (Δε + 0.23), 232 (Δε – 0.22), 289 (Δε + 0.09) nm; (+)-HR-ESI-MS *m/z* 635.2464 [M+Na]⁺ (calcd. for C₃₃H₄₀O₁₁Na, 635.2468).

2.5. Cell culture

RAW 264.7 macrophages were purchased from the Shanghai Cell Bank of the Chinese Academy of Sciences and cultured in DMEM containing 10% FBS, 100 U/mL penicillin, and 100 μg/mL streptomycin at 37 °C in a humidified atmosphere with 5 % CO₂.

2.6. Anti-inflammatory activity assay

The doses of the tested compounds were chosen according to a cell viability assay in normal RAW 264.7 cells using CCK-8 kits. Then, in the anti-inflammatory assay, RAW 264.7 cells were seeded in a 96-well plate (5 × 10⁴ cells per well) and incubated for 24 h. Subsequently, the cells were treated with 1 μg/mL LPS for 24 h with or without various concentrations of tested compounds (curcumin was used as a positive control) (Huang et al., 2022, Li et al., 2021). Then, the supernatants were collected and assayed for NO production with an NO kit using Griess reagent. Absorbance was measured using a microplate reader at a wavelength of 570 nm. NO levels in samples were determined based on a standard curve.

2.7. Western blot analysis

RAW 264.7 cells were pretreated with compound **3a** (12.5, 25, and 50 μM) for 1 h and then stimulated with 1 $\mu\text{g}/\text{mL}$ LPS. To obtain total proteins, the cells were lysed in RIPA buffer containing proteinase inhibitors and crushed with an ultrasonic cell pulverizer. Equal quantities of protein (30 μg per lane) were separated using SDS-PAGE and transferred to PVDF membranes, which were blocked in 5% non-fat milk for 2 h at room temperature and incubated with primary antibodies against ERK, p-ERK, NF- κB , p-NF- κB , iNOS, and β -actin overnight at 4 $^{\circ}\text{C}$. After three washes with TBST, membranes were incubated with HRP-conjugated goat anti-rabbit secondary antibodies for 1 h at room temperature and washed again. Protein bands were visualized by enhanced chemiluminescence. Western blot images were captured using a Tanon 5200 chemiluminescence imaging system.

2.8. Statistical analysis

Data are presented as mean \pm standard deviation (SD). All experiments were conducted at least three times. One-way analysis of variance was conducted for comparisons among multiple groups, and the least significant difference test was used for comparisons between two groups. Figures were prepared using GraphPad Prism version 5.0 (GraphPad Software, Inc., San Diego, CA, US). In all comparisons, $P < 0.05$ was considered statistically significant.

3. Results

3.1. Inhibitory effect of AWSF on NO production in RAW 264.7 cells

To exclude the possibility that the cytotoxicity of AWSF may contribute to its anti-inflammatory effect, the viability of RAW 264.7 cells treated with various AWSF concentrations was evaluated using the CCK-8 assay. As shown in Fig. 2A, AWSF exhibited no cytotoxic effect at concentrations of 6.25, 12.5, 25, 50, and 100 $\mu\text{g}/\text{mL}$. Therefore, it is rational to apply these concentrations in the subsequent experiments.

Because overproduction of NO is a typical marker for inflammation in activated macrophages, Griess reagent kits were applied to assess extracellular NO concentrations. As presented in Fig. 2B, NO production in RAW 264.7 macrophages was markedly increased by stimulation with LPS, and AWSF could significantly decrease the NO content in a dose-dependent manner with an IC_{50} value of 14.59 $\mu\text{g}/\text{mL}$.

3.2. AWSF decreased the protein expression of p-ERK and iNOS in LPS-activated RAW 264.7 cells

NO, a pro-inflammatory mediator, is synthesized excessively by iNOS when macrophages are stimulated by LPS (Feng et al., 2021, Xiang et al., 2018). Thus, we speculated that iNOS might be involved in the effect of AWSF on NO release. In addition, numerous studies have reported that ERK, a member of the MAPK family, is critical for activating NF- κB , which could subsequently activate iNOS expression (Peng et al., 2015, Zou et al., 2018). Considering that AWSF is a mixture, it is acceptable to preliminarily explore whether AWSF decreases NO overproduction by suppressing ERK and iNOS protein expression. As shown in Fig. 3, AWSF suppressed LPS-activated protein expression of p-ERK and iNOS in a dose-dependent manner, indicating that AWSF may exert anti-inflammatory activity by inhibiting p-ERK and iNOS expression.

3.3. Structure elucidation of the compounds isolated from AWSF

Compound **1** was obtained as a white powder. HR-ESI-MS analysis of **1** gave an $[\text{M}+\text{Na}]^+$ at m/z 797.2995 revealing a molecular formula of $\text{C}_{39}\text{H}_{50}\text{O}_{16}$ (calcd. for $\text{C}_{39}\text{H}_{50}\text{O}_{16}\text{Na}$, 797.2997). The IR spectrum of **1** displayed strong signals at 1634, 1567, 1514, and 3296 cm^{-1} , supporting the presence of aromatic rings and hydroxy groups. To provide more detailed structural information, the ^1H NMR spectrum (Table 1) displayed typical signals that corresponded to two 1,3,4-trisubstituted aromatic rings [δ_{H} 6.90 (1H, d, $J=1.8$ Hz), 6.90 (1H, d, $J=8.4$ Hz), 6.82 (1H, dd, $J=8.4, 1.8$ Hz), 6.81 (1H, d, $J=8.4$ Hz), 6.76 (1H, d, $J=1.8$ Hz), and 6.66 (1H, dd, $J=8.4, 1.8$ Hz)], a 1,3,4,5-tetrasubstituted aromatic ring [δ_{H} 6.56 (2H, br.s)], two exchangeable aromatic hydroxy protons (δ_{H} 5.62 and 5.56), four aromatic methoxy groups (δ_{H} 3.91, 3.84, and 3.83), multiple oxygenated methylene and methine groups, two non-oxygenated methine groups, and a methyl group. The ^{13}C NMR data (Table 1) in combination with DEPT and HSQC spectra exhibited carbon signals corresponding to the above protons, including 19 methine signals [eight aromatic (δ_{C} 120.2, 119.1, 114.4, 114.2, 109.2, 108.7, 103.4, 103.4), nine oxygenated (δ_{C} 104.1, 86.1, 85.9, 85.7, 81.2, 76.6, 75.3, 74.0, 70.5), and two non-oxygenated (δ_{C} 54.6, 54.2)], five oxygenated methylene signals (δ_{C} 72.2, 71.7, 69.5, 65.3, 62.6), and five methyl signals [a methyl group (δ_{C} 15.6) and four methoxy groups (δ_{C} 56.4, 56.4, 56.1, 56.1)]. In addition, the ^{13}C NMR and DEPT data indicated the presence of 10 aromatic quaternary carbons attributed to three phenyl units. From the above data, it can be seen that **1** contains three C6-C3 moieties substituted with four aromatic methoxy groups, two phenolic hydroxy groups, and a glycosyl group. Moreover, according to the coupling constant of the anomeric proton ($J=7.8$ Hz) and the ^{13}C

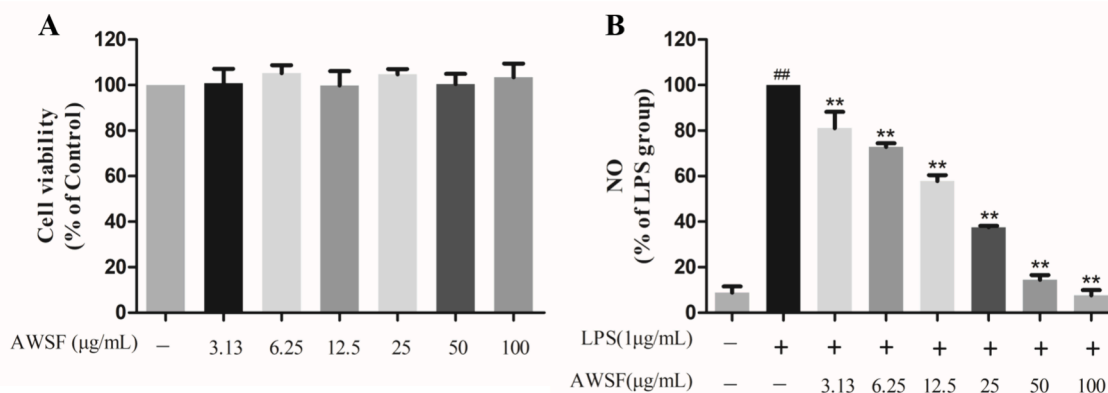


Fig. 2. Inhibitory effect of AWSF on LPS-induced NO production in RAW 264.7 cells. (A) Effect of AWSF on the survival rate of normal macrophages. (B) Effect of AWSF on NO release from macrophages. Data are shown as mean \pm SD of three independent experiments. ### $P < 0.01$ vs. untreated control; ** $P < 0.01$ vs. model group.

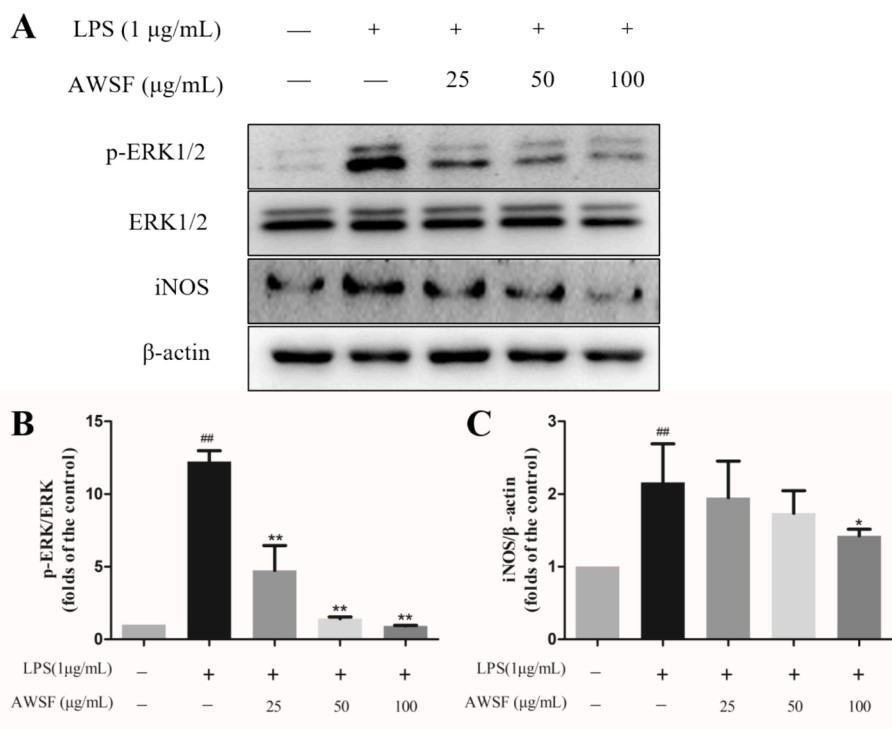


Fig. 3. Effect of AWSF on the expression of inflammatory-related proteins. (A) Expression levels of p-ERK1/2 (Thr202/Tyr204) and iNOS. (B) p-ERK/ERK ratio. (C) iNOS/ β -actin ratio. Data are shown as mean \pm SD. $##P < 0.01$ vs. untreated control; $*P < 0.05$ and $**P < 0.01$ vs. model group ($n = 3$).

chemical shifts of the sugar moiety, it is inferred that there is a β -glucopyranosyl (Xiong et al., 2013). Therefore, compound **1** is a sesquieolignan β -glucopyranoside.

A rigorous survey of the literature revealed that **1** and (–)-(7*R*,7'*R*,7''*R*,8*S*,8'*S*,8''*S*)-4',4''-dihydroxy-3,3',3'',5-tetramethoxy-7,9':7',9'-diepoxy-4,8'-oxy-8,8'-sesquieolignan-7'',9''-diol (Xiong et al., 2011) have a very similar sesquieolignan skeleton, both of which are linked by medioresinol and guaiacylglycerol. The main difference is that **1** has one more β -glucopyranosyl unit and an ethoxy group than the compound reported in the literature. Detailed comparison of the ^{13}C NMR data between the two compounds showed that C-7'' and C-9'' resonances in **1** were shifted by $\Delta\delta_{\text{C}}+8.7$ and $+8.8$ ppm, respectively, indicating that the β -glucopyranosyl and ethoxy groups are attached at the C-7'' and C-9'' positions. The inference of the planar structure of **1** was confirmed by 2D NMR including ^1H - ^1H COSY, HSQC, and HMBC (Fig. 4). In the HMBC spectrum, H-7 shared correlations with C-9, C-8', and C-9', while H-7' displayed correlations with C-8, C-9, and C-9', in

combination with the COSY correlations of H-7/H-8/H₂-9, H-7'/H-8'/H₂-9', and H-8/H-8', confirming the existence of the tetrahydrofuran ring in **1**. Two symmetric methoxy groups are connected to the C-3 and C-5 positions based on the HMBC correlations of H-2/6 with C-1, C-3/5, C-4, and C-7, as well as OMe-3/5 with C-3/5. A methoxy group and a hydroxy group were determined to be located at the C-3' and C-4' positions, relying on the correlations from H-5' to C-1', C-3', and C-6'; from H-6' to C-2' and C-4'; from OMe-3' to C-3'; from OH-4' to C-3', C-4', and C-5'; and from H-8' to C-1', C-2', and C-3'. Similarly, it can be determined that a methoxy group and a hydroxy group were attached to C-3'' and C-4'', respectively. Furthermore, according to the HMBC correlations of H-7'' with C-1'', C-2'', C-6'', C-8'', and C-9'', together with the COSY correlations of H-7''/H-8''/H₂-9'', it is inferred that **1** contains a guaiacylglycerol fragment. The ethoxyl group at C-7'' was established by the HMBC correlation of H-7'' with C-10'', while the β -glucopyranosyl group was connected to C-9'' based on the HMBC correlation of H-1'' with C-9''. Although no HMBC signal for the ether bond between H-8''

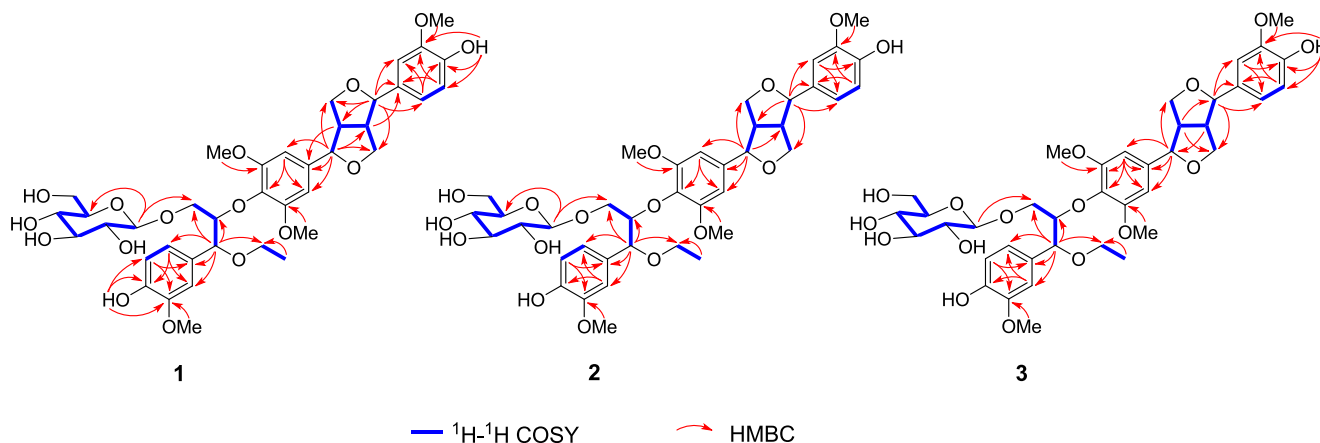


Fig. 4. Key HMBC and ^1H - ^1H COSY correlations of compounds **1**–**3**.

and C-4 was observed, the connection of 8''-O-4 can be inferred from the molecular formula and the chemical shifts of H-8'' (δ_{H} 4.36), C-8'' (δ_{C} 85.7), and C-4 (δ_{C} 135.5). Therefore, the planar structure of **1** was determined as 4',4''-dihydroxy-3,3',3'',5-tetramethoxy-7''-ethoxy-7,9':7',9'-diepoxy-4,8''-oxy-8,8'-sesquieolignan-9''-O- β -D-glucopyranoside.

The relative configuration of **1** was determined through a comprehensive analysis of coupling constants, chemical shifts, and NOESY data. First, the ^1H NMR and ^{13}C NMR shifts for the bis-tetrahydrofuran ring in **1** were analyzed, revealing that both H-7 and H-7' were at 4.6–5.1 ppm, H-8 and H-8' at 3.0–3.2 ppm, H-9a and H-9'a at 4.2–4.4 ppm, H-9b and H-9'b at 3.8–4.0 ppm, C-7 and C-7' at 82–87 ppm, C-8 and C-8' at 54–56 ppm, and C-9 and C-9' at 71–74 ppm. According to empirical rules (Xiong et al., 2011, Shi, 2009, Greger and Hofer, 1980), it can be deduced that the bis-tetrahydrofuran lignan fragment of **1** is of the *eq/eq* type, and H-7/H-8 and H-7'/H-8' are in *trans* orientation. These relative configurations can further be confirmed by $\Delta\delta_{\text{H-9a, 9b}}$ (0.35 ppm) and $\Delta\delta_{\text{H-9'a, 9'b}}$ (0.39 ppm) (Shao et al., 2018), both of which were in the range of 0.3–0.4 ppm. The above inference is also consistent with the NOESY data of **1**, in which H-2/6 showed correlations to H-8, while H-2'/H-6' shared correlations with H-8'. Regarding the guaiacylglycerol fragment, the relative configuration was determined by the coupling constant of H-7'' and H-8'' ($J_{7'',8''}$). According to the empirical rules for 8,4'-oxolignans, $J_{7'',8''}$ can be used for the determination of their relative configurations and is influenced by the tested solvent (Xiong et al., 2011, Gan et al., 2008). Therefore, the guaiacylglycerol unit of **1** was inferred to be an *erythro* configuration based on $J_{7'',8''} = 3.6$ Hz (CDCl_3).

To further determine the absolute configuration, compound **1** was enzymatically hydrolyzed to obtain aglycone **1a** (Table 2) and a glucose. The glucose was identified as D-glucose using TLC and $[\alpha]_{\text{D}}^{20}$ compared with a D-glucose reference standard (Xiong et al., 2013, Husdon and Dale, 1916). Because the cotton peaks in ECD spectra are widely used to determine the absolute configurations of lignans, the ECD data of **1** were measured. Numerous studies have shown that in 8,4'-oxyneolignans, the Cotton effect at 230–240 nm can be used to determine the configuration of C-8 in the aryl glycerol units (positive for 8S and negative for 8R) (Xiong et al., 2011, Gan et al., 2008, Huo et al., 2008, Greca et al., 1994), while in the *eq/eq*-type 7,9':7',9'-diepoxyneolignans, the Cotton effect at around 280 nm can be validated for the configuration assignment of the bis-tetrahydrofuran ring (positive for 7S,7'S,8R,8'R and negative for 7R,7'R,8S,8'S) (Shi, 2009, Hofer and Schölm, 1981, Hosokawa et al., 2004). However, in the sesquieolignans with a bis-tetrahydrofuran ring and an aryl glycerol unit, these empirical rules could not be applied to determine the absolute configuration of the aryl glycerol unit but could be used only for configuration determination of the bis-tetrahydrofuran lignan fragment. This is because the bis-tetrahydrofuran lignan fragment could also generate an obvious Cotton effect at 230–245 nm in addition

to the Cotton effect at around 280 nm (Hofer and Schölm, 1981; Hosokawa et al., 2004; Muhit et al., 2016; Li et al., 2008,2014), which means that the Cotton effect at 230–245 nm of such sesquieolignans is caused by a comprehensive effect of the aryl glycerol unit and the bis-tetrahydrofuran lignan fragment. In this study, to begin with, a positive Cotton effect at 279 nm ($\Delta\epsilon + 0.41$) indicated that the *eq/eq*-type bis-tetrahydrofuran lignan fragment in **1a** had a 7S,7'S,8R,8'R configuration. Then, the absolute configuration of the guaiacyl glycerol unit in **1a** was determined through ECD calculations, using the time-dependent density functional theory method. Based on the *erythro* relative configuration of the guaiacyl glycerol unit, the absolute configuration of C-7'' and C-8'' might be 7''S,8''R or 7''R,8''S. Thus, compound **1a** could be inferred as (7S,7'S,7''S,8R,8'R,8''R)-**1a** or (7S,7'S,7''R,8R,8'R,8''S)-**1a**. ECD calculations showed that the experimental ECD spectrum of **1a** matched the calculated ECD spectrum of (7S,7'S,7''S,8R,8'R,8''R)-**1a** (Fig. 5). Consequently, the structure of **1** was determined as (-)-(7S,7'S,7''S,8R,8'R,8''R)-4',4''-dihydroxy-3,3',3'',5-tetramethoxy-7''-ethoxy-7,9':7',9'-diepoxy-4,8''-oxy-8,8'-sesquieolignan-9''-O- β -D-glucopyranoside (named leolignoside A).

Compound **2** showed very similar spectroscopic data to those of **1**, indicating that **2** is also a sesquieolignan derivative with a similar structure. HR-ESI-MS displayed that **2** had the same molecular formula as **1** ($\text{C}_{39}\text{H}_{50}\text{O}_{16}$), thus **2** was inferred to be an isomer of **1**. Detailed comparison of the ^1H and ^{13}C NMR data between **2** and **1** (Table 1) revealed that the most prominent difference is that C-8'' resonance in **2** was shifted by $\Delta\delta_{\text{C}} - 2.4$ ppm, while the coupling constant of H-7'' and H-8'' ($J_{7'',8''}$) in **2** was increased to 6.0 Hz. Thus, it can be assumed that **2** is the C-8'' epimer of **1**. 2D NMR data analysis further verified that **2** had the same planar structure as **1** (Fig. 1). Moreover, based on ^1H and ^{13}C NMR data of the bis-tetrahydrofuran ring, it was clear that the bis-tetrahydrofuran lignan fragment of **2** was also of the *eq/eq* type. In particular, $\Delta\delta_{\text{H-9a, 9b}}$ and $\Delta\delta_{\text{H-9'a, 9'b}}$ (0.3–0.4 ppm) (Shao et al., 2018), together with the NOESY correlations of H-2/H-6 with H-8 and H-2'/H-6' with H-8', confirmed it was of the *eq/eq* type. The relative configuration of the guaiacyl glycerol fragment was determined as *threo* according to the coupling constant of $J_{7'',8''} = 6.6$ Hz (Xiong et al., 2011, Gan et al., 2008).

Using the same methods as described for **1**, compound **2** was enzymatically hydrolyzed to obtain its aglycone **2a** (Table 2) and a D-glucose. The ECD spectrum of **2a** showed a positive Cotton effect at 282 nm, similar to that of **1a**, indicating that the *eq/eq*-type bis-tetrahydrofuran lignan fragment of **2a** was also a 7S,7'S,8R,8'R configuration. Then, compound **2a** was assumed as (7S,7'S,7''S,8R,8'R,8''S)-**2a** or (7S,7'S,7''R,8R,8'R,8''R)-**2a** for ECD calculation according to the above *threo* configuration of the guaiacyl glycerol unit. As shown in Fig. 5, the calculated ECD spectrum of (7S,7'S,7''S,8R,8'R,8''S)-**2a** agreed with the

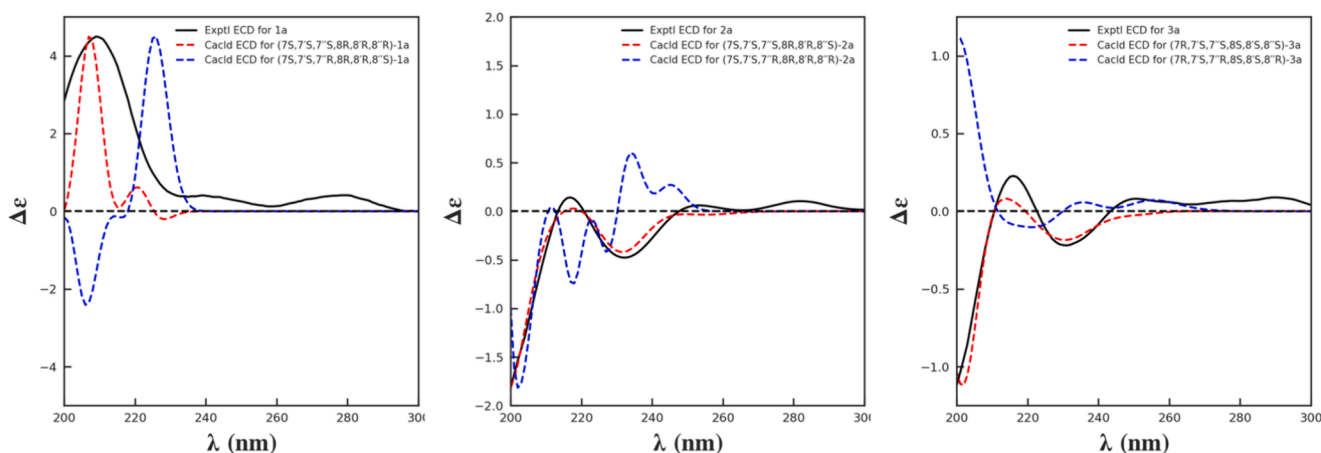


Fig. 5. Experimental and calculated ECD spectra of compounds **1a–3a**.

experimental ECD spectrum of **2a**. Therefore, compound **2** was determined to be $(-)-(7S,7'S,7''S,8R,8'R,8''S)-4',4''$ -dihydroxy-3,3',3''-5-tetramethoxy-7''-ethoxy-7,9':7',9''-diepoxy-4,8'-oxy-8,8'-sesquieolignan-9''-O- β -D-glucopyranoside (leolignoside B).

Compound **3** showed similar spectroscopic data and the same molecular formula as **1** and **2**, inferring that **3** may be a sesquieolignan glycoside analog with the same planar structure. This deduction was demonstrated through 2D NMR experiments. Further comparison of ^1H and ^{13}C NMR data of **3** and **2** uncovered that the resonance signals of the guaiaacyl glycerol β -D-glucopyranoside fragment in **3** and **2** were almost the same, including the chemical shifts and coupling constants. Thus, the relative configuration of the guaiaacyl glycerol unit in **3** was also *threo*. Applying empirical rules (Shi, 2009; Greger and Hofer, 1980), the ^1H and ^{13}C NMR data of the bis-tetrahydrofuran ring in **3** indicated that the bis-tetrahydrofuran lignan unit is not of the *eq/eq* type but of the *eq/ax* type. The relative configuration was further verified by $\Delta\delta_{\text{H-9a, 9b}}$ (0.27 ppm, in the range of 0.205–0.36 ppm) and $\Delta\delta_{\text{H-9'a, 9'b}}$ (0.52 ppm > 0.50 ppm) (Shao et al., 2018). After enzyme hydrolysis of **3**, the aglycone **3a** (Table 2) and a D-glucose were obtained. In the ECD spectrum of **3a**, a positive Cotton effect at 289 nm suggested that the *eq/ax*-type bis-tetrahydrofuran lignan fragment of **3a** has a $7R,7'S,8S,8'S$ configuration (Muhit et al., 2016; Li et al., 2008; Li et al., 2014). Then, two possible isomers, $(7R,7'S,7''R,8S,8'S,8''R)-3a$ and $(7R,7'S,7''S,8S,8'S,8''S)-3a$, were applied to ECD calculations. The results showed that $7R,7'S,7''S,8S,8'S,8''S$ was the most probable configuration for **3a** (Fig. 5). Accordingly, compound **3** was determined to be $(-)-(7R,7'S,7''S,8S,8'S,8''S)-4',4''$ -dihydroxy-3,3',3''-5-tetramethoxy-7''-ethoxy-7,9':7',9''-diepoxy-4,8'-oxy-8,8'-sesquieolignan-9''-O- β -D-glucopyranoside (leolignoside C).

3.4. Inhibitory effects of compounds **1a–3a** on NO production in RAW 264.7 cells

Similar to AWSF, compounds **1a–3a** were first evaluated for their cytotoxic effects in RAW 264.7 cells. As presented in Fig. 6A, these

compounds all showed no cytotoxicity at concentrations of 12.5, 25, and 50 μM , which provided evidence for further anti-inflammatory assessments.

The results shown in Fig. 6B reveal that sesquieolignans **1a, 2a,** and **3a** exerted inhibitory effects on NO release in LPS-injured RAW 264.7 cells. The IC_{50} values of **2a** and **3a** was 22.67 and 33.58 μM , respectively. Curcumin was used as a positive control ($\text{IC}_{50} = 27.90 \mu\text{M}$). Although compound **2a** showed the most potent effect, its inhibitory effect on inflammatory-related protein expression was not investigated because the amount of sample available was low. Compound **3a** was selected for the subsequent experiments.

3.5. Inhibitory effect of compound **3a** on p-ERK and p-NF- κB expression in LPS-injured RAW 264.7 cells

Based on the preliminary exploration of AWSF, the inhibitory effect of compound **3a** on protein expression was also examined. As shown in Fig. 7, the LPS-induced increase in p-ERK and p-NF- κB was reversed by **3a**. However, unfortunately, iNOS expression was not investigated due to the limited amount of **3a**. In summary, compound **3a** exerted anti-inflammatory activity through the ERK/NF- κB signaling pathway.

4. Discussion

It is difficult to determine the configurations of lignans, especially for sesquieolignans, due to their multiple chiral centers on the rings and the chains. Over the years, researchers have attempted to solve this problem, and some empirical rules have been summarized. In the 7,9':7',9''-diepoxy lignans, the relative configuration of the bis-tetrahydrofuran ring could be determined through NOE data analysis coupled with empirical rules of the ^1H and ^{13}C NMR data (Shi, 2009; Greger and Hofer, 1980; Shao et al., 2018). Particularly, $\Delta\delta_{\text{H-9a, 9b}}$ and $\Delta\delta_{\text{H-9'a, 9'b}}$ are available for the determination of the relative configuration (*eq/eq* type: $\Delta\delta_{\text{H-9a, 9b}}$ and $\Delta\delta_{\text{H-9'a, 9'b}}$ in the range of 0.3–0.4 ppm; *eq/ax* type: $\Delta\delta_{\text{H-9a, 9b}}$ in the range of 0.205–0.36 ppm, $\Delta\delta_{\text{H-9'a, 9'b}} > 0.50$

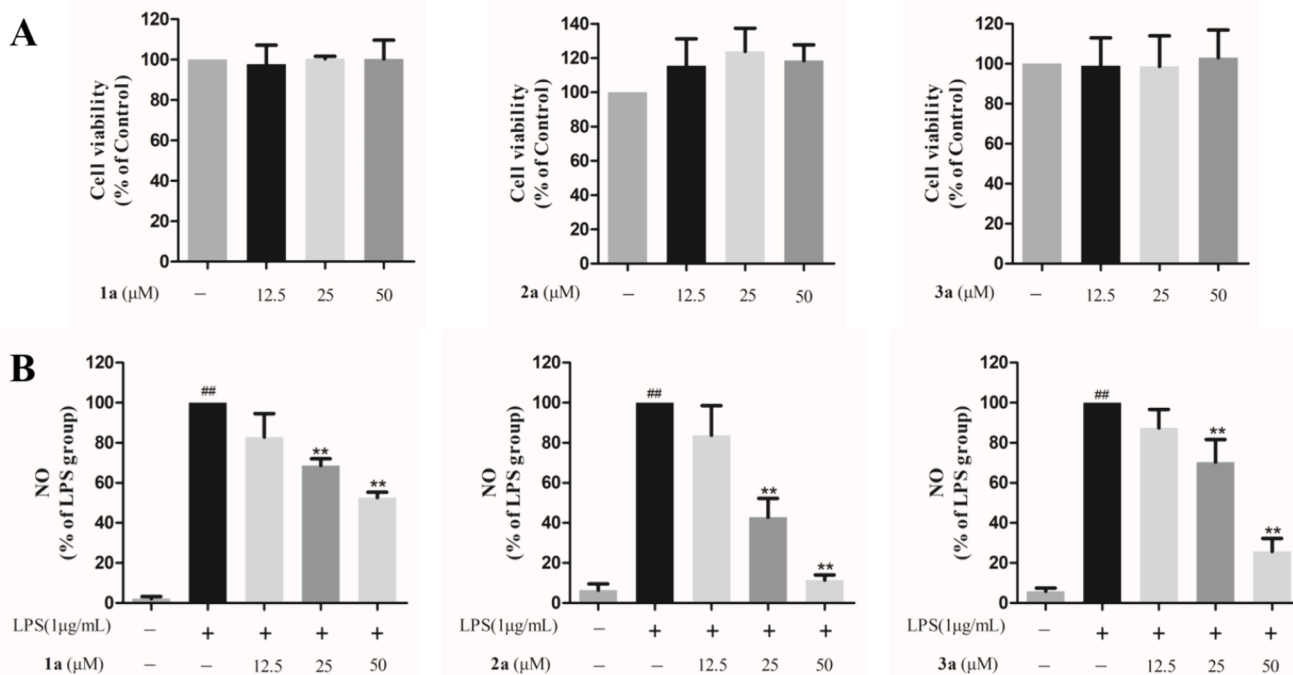


Fig. 6. Effects of compounds **1a–3a** on NO release from macrophages. (A) Effects of compounds **1a–3a** on the survival rate of normal macrophages. (B) Effects of compounds **1a–3a** on NO release from macrophages. Data are shown as mean \pm SD of three independent experiments. $\#\#P < 0.01$ vs. untreated control; $\#\#\#P < 0.01$ vs. model group.

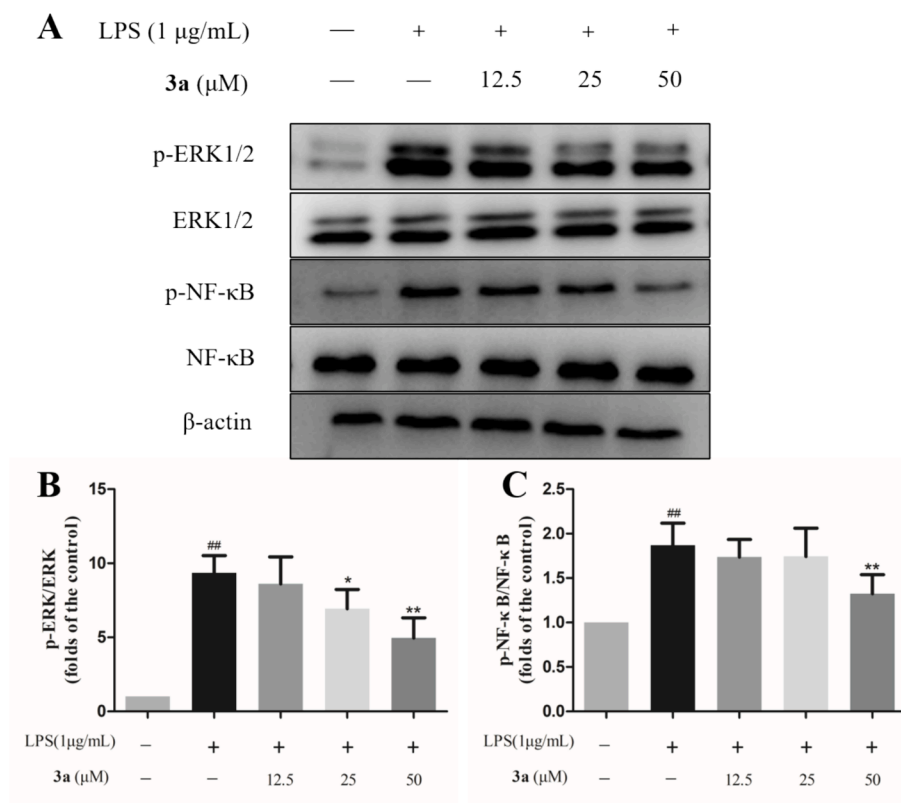


Fig. 7. Effect of compound **3a** on the expression of inflammation-related proteins. (A) Expression levels of p-ERK1/2 (Thr202/Tyr204) and p-NF-κB (Ser536). (B) p-ERK/ERK ratio. (C) p-NF-κB/NF-κB ratio. Data are shown as mean \pm SD. ^{##} $P < 0.01$ vs. untreated control; ^{*} $P < 0.05$ and ^{**} $P < 0.01$ vs. model group (n = 3).

ppm) (Shao et al., 2018). For determination of the bis-tetrahydrofuran moiety, the Cotton effect at around 280 nm was often applied (*eq/eq* type: positive for 7*S*,7*S*,8*R*,8*R* and negative for 7*R*,7*R*,8*S*,8*S*; *eq/ax* type: positive for 7*R*,7*S*,8*S*,8*S* and negative for 7*S*,7*R*,8*R*,8*R*) (Shi, 2009; Hofer and Schölm, 1981; Hosokawa et al., 2004; Muhit et al., 2016; Li et al., 2008; Li et al., 2014). Regarding 8,4'-oxyneolignans with an aryl glycerol unit, the coupling constant of H-7 and H-8 ($J_{7,8}$) is widely used to determine the relative configuration (*erythro* type: $J_{7,8} \leq 4.0$ Hz; *threo* type: $J_{7,8} \geq 6.0$ Hz) (Xiong et al., 2011; Gan et al., 2008). When it comes to the absolute configuration of the aryl glycerol unit, the Cotton effect at 230–240 nm in the ECD spectrum is usually applied (positive for 8*S* and negative for 8*R*) (Xiong et al., 2011; Gan et al., 2008; Huo et al., 2008; Greca et al., 1994). However, for the sesqueneolignans with a bis-tetrahydrofuran lignan fragment and an aryl glycerol unit, the Cotton effect at 230–240 nm is contributed by both the aryl glycerol and 7,9':7',9'-diepoxy lignan chromophores in the molecules. Thus, the above empirical rules are not suitable for determining the absolute configuration of aryl glycerol units in sesqueneolignans. In the present study, to determine the complicated absolute configuration of sesqueneolignan glycosides, coupling constants, NOESY data, empirical rules, enzymatic hydrolysis, and ECD data were comprehensively used, which made the conclusion more reliable.

5. Conclusions

In the present study, we discovered that the AWSF of the 95 % EtOH extract of *L. japonicus* had significant anti-inflammatory activity by suppressing NO overproduction and iNOS and p-ERK expression in LPS-activated macrophages. Then, the chemical composition of AWSF was investigated. Three new sesqueneolignan glycosides were isolated, and their complicated absolute configurations were determined based on coupling constants, NOESY data, empirical rules, enzymatic hydrolysis, and ECD data. All sesqueneolignan aglycones showed anti-inflammatory

activities, and **3a** was chosen for further study. The results suggest that **3a** may decrease NO production through the ERK/NF-κB signaling pathway.

CRediT authorship contribution statement

Lan Bu: Investigation, Writing – original draft. **Qin-Mei Zhou:** Investigation, Writing – original draft. **Cheng Peng:** Methodology, Project administration. **Hong-Zhen Shu:** Investigation. **Fei Zhou:** Data curation, Methodology. **Guang-Xu Wu:** Investigation. **Fei Liu:** Data curation, Methodology. **Hui Tian:** Supervision, Writing – review & editing. **Liang Xiong:** Funding acquisition, Supervision, Writing – review & editing.

Declaration of competing interest

The authors declare that they have no known competing financial interests or personal relationships that could have appeared to influence the work reported in this paper.

Acknowledgments

This work was supported by the National Natural Science Foundation of China (Grant Nos. 82022072 and 81872991), the Innovation Team Program of Jinan City (Grant No. 202228038), and “Xinglin Scholar” Plan of Chengdu University of Traditional Chinese Medicine (Grant No. XKTD2022006).

Appendix A. Supplementary data

Supplementary data to this article can be found online at <https://doi.org/10.1016/j.arabjc.2024.105932>.

References

- Feng, Z., Chen, J., Feng, L., Chen, C., Ye, Y., Lin, L., 2021. Polyisoprenylated benzophenone derivatives from *Garcinia cambogia* and their anti-inflammatory activities. *Food Funct.* 12, 6432–6441. <https://doi.org/10.1039/d1fo00972a>.
- Gan, M., Zhang, Y., Lin, S., Liu, M., Song, W., Zi, J., Yang, Y., Fan, X., Shi, J., Hu, J., Sun, J., Chen, N., 2008. Glycosides from the root of *Iodes cirrhosa*. *J. Nat. Prod.* 71, 647–654. <https://doi.org/10.1021/np7007329>.
- Greca, M.D., Molinaro, A., Monaco, P., Previtera, L., 1994. Lignans from *Arum italicum*. *Phytochemistry* 35, 777–779. [https://doi.org/10.1016/S0031-9422\(00\)90604-6](https://doi.org/10.1016/S0031-9422(00)90604-6).
- Greger, H., Hofer, O., 1980. New unsymmetrically substituted tetrahydrofuran lignans from *Artemisia absinthium*. *Tetrahedron* 36, 3551–3558. [https://doi.org/10.1016/0040-4020\(80\)88051-3](https://doi.org/10.1016/0040-4020(80)88051-3).
- Hofer, O., Schölm, R., 1981. Stereochemistry of tetrahydrofuran derivatives—circular dichroism and absolute configuration. *Tetrahedron* 37, 1181–1186. [https://doi.org/10.1016/S0040-4020\(01\)92047-2](https://doi.org/10.1016/S0040-4020(01)92047-2).
- Hosokawa, A., Sumino, M., Nakamura, T., Yano, S., Sekine, T., Ruangrungrui, N., Watanabe, K., Ikegami, F., 2004. A new lignan from *Balanophora abbreviata* and inhibition of lipopolysaccharide (LPS)-induced inducible nitric oxide synthase (iNOS) expression. *Chem. Pharm. Bull.* 52, 1265–1267. <https://doi.org/10.1248/cpb.52.1265>.
- Huang, L., Peng, C., Guo, L., Feng, R., Shu, H.Z., Tian, Y.C., Zhou, Q.M., Xiong, L., 2022. Six pairs of enantiomeric phthalide dimers from the rhizomes of *Ligusticum chuanxiong* and their absolute configurations and anti-inflammatory activities. *Bioorg. Chem.* 127, 105970. <https://doi.org/10.1016/j.bioorg.2022.105970>.
- Huo, C., Liang, H., Zhao, Y., Wang, B., Zhang, Q., 2008. Neolignan glycosides from *Symplocos caudata*. *Phytochemistry* 69, 788–795. <https://doi.org/10.1016/j.phytochem.2007.08.022>.
- Husdon, C.S., Dale, J.K., 1916. Studies on the forms of D-glucose and their mutarotation. *J. Am. Chem. Soc.* 889, 320–328. <https://doi.org/10.1021/ja02247a017>.
- Li, T., Hao, X.J., Gu, Q.Q., Zhu, W.M., 2008. Minor furofuran lignans from the Tibetan herb, *Lancea tibetica*. *Planta Med.* 74, 1391–1396. <https://doi.org/10.1055/s-2008-1081308>.
- Li, X.R., Liu, J., Peng, C., Zhou, Q.M., Liu, F., Guo, L., Xiong, L., 2021. Polyacetylene glycosides from the florets of *Carthamus tinctorius* and their anti-inflammatory activity. *Phytochemistry* 187, 112770. <https://doi.org/10.1016/j.phytochem.2021.112770>.
- Li, Z.L., Yang, M.S., Peng, Y., Gao, M., Yang, B.C., 2019. Rutaecarpine ameliorated sepsis-induced peritoneal resident macrophages apoptosis and inflammation responses. *Life Sci.* 228, 11–20. <https://doi.org/10.1016/j.lfs.2019.01.038>.
- Li, C., Yao, Z.H., Qin, Z.F., Zhang, J.B., Cao, R.Y., Dai, Y., Yao, X.S., 2014. Isolation and identification of phase I metabolites of phillyrin in rats. *Fitoterapia* 97, 92–97. <https://doi.org/10.1016/j.fitote.2014.05.011>.
- Liu, J., Peng, C., Zhou, Q.M., Guo, L., Liu, Z.H., Xiong, L., 2018. Alkaloids and flavonoid glycosides from the aerial parts of *Leonurus japonicus* and their opposite effects on uterine smooth muscle. *Phytochemistry* 145, 128–136. <https://doi.org/10.1016/j.phytochem.2017.11.003>.
- Macías, F.A., López, A., Varela, R.M., Torres, A., Molinillo, J.M.G., 2004. Bioactive lignans from a cultivar of *Helianthus annuus*. *J. Agric. Food Chem.* 52, 6443–6447. <https://doi.org/10.1021/jf048945d>.
- Miao, L.L., Zhou, Q.M., Peng, C., Liu, Z.H., Xiong, L., 2019. *Leonurus japonicus* (Chinese motherwort), an excellent traditional medicine for obstetrical and gynecological diseases: a comprehensive overview. *Biomed. Pharmacother.* 117, 109060. <https://doi.org/10.1016/j.biopha.2019.109060>.
- Muhtit, M.A., Umehara, K., Mori-Yasumoto, K., Noguchi, H., 2016. Furofuran lignan glycosides with estrogen-inhibitory properties from the Bangladeshi medicinal plant *Terminalia citrina*. *J. Nat. Prod.* 79, 1298–1307. <https://doi.org/10.1021/acs.jnatprod.5b01042>.
- Peng, F., Xiong, L., Zhao, X.M., 2013. A bicyclic diterpenoid with a new 15,16-dinor-labdane carbon skeleton from *Leonurus japonicus* and its coagulant bioactivity. *Molecules* 18, 13904–13909. <https://doi.org/10.3390/molecules181113904>.
- Peng, F., Xiong, L., He, Y.L., Liu, F., Peng, C., 2021. 8-O-4' Neolignans from the fruits of *Leonurus japonicus*. *Nat. Prod. Res.* Dev. 2021 (33), 1320–1325. <https://doi.org/10.16333/j.1001-6880.2021.8.007>.
- Peng, X.X., Zhang, S.H., Wang, X.L., Ye, T.J., Li, H., Yan, X.F., Wei, L., Wu, Z.P., Hu, J., Zou, C.P., Wang, Y.H., Hu, X.D., 2015. *Panax notoginseng* flower saponins (PNFS) inhibit LPS-stimulated NO overproduction and iNOS gene overexpression via the suppression of TLR4-mediated MAPK/NF-kappa B signaling pathways in RAW264.7 macrophages. *Chin. Med. (United Kingdom)* 10, 1–11. <https://doi.org/10.1186/s13020-015-0045-x>.
- Shao, S.Y., Yang, Y.N., Feng, Z.M., Jiang, J.S., Zhang, P.C., 2018. An efficient method for determining the relative configuration of furofuran lignans by ¹H NMR spectroscopy. *J. Nat. Prod.* 81, 1023–1028. <https://doi.org/10.1021/acs.jnatprod.8b00044>.
- Shi, J.G., 2009. Lignan chemistry. *Chem. Ind. Press* 55–56.
- Sun, H.J., Cai, W.W., Wang, X., Liu, Y.L., Hou, B., Zhu, X.X., Qiu, L.Y., 2017. *Vaccaria hypaphorine* alleviates lipopolysaccharide-induced inflammation via inactivation of NFκB and ERK pathways in Raw 264.7 cells. *BMC Compl. Altern. Med.* 1, 120. <https://doi.org/10.1186/s12906-017-1635-1>.
- Tian, Z.H., Liu, F., Peng, F., He, Y.L., Shu, H.Z., Lin, S., Chen, J.F., Peng, C., Xiong, L., 2021. New lignans from the fruits of *Leonurus japonicus* and their hepatoprotective activities. *Bioorg. Chem.* 115, 105252. <https://doi.org/10.1016/j.bioorg.2021.105252>.
- Xiang, L., Hu, Y.F., Wu, J.S., Wang, L., Huang, W.G., Xu, C.S., Meng, X.L., Wang, P., 2018. Semi-mechanism-based pharmacodynamic model for the anti-inflammatory effect of baicalin in LPS-stimulated RAW264.7 macrophages. *Front. Pharmacol.* 9, 1–9. <https://doi.org/10.3389/fphar.2018.00793>.
- Xiong, L., Cai, L.Y., Tian, Y., Lin, S., Yuan, S., Hu, J., Hou, Q., Chen, N., Yang, Y., Shi, J., 2011. Lignans and neolignans from *Sinocalamus affinis* and their absolute configurations. *J. Nat. Prod.* 74, 1188–1200. <https://doi.org/10.1021/np200117y>.
- Xiong, L., Cao, Z.X., Peng, C., Li, X.H., Xie, X.F., Zhang, T.M., Zhou, Q.M., Yang, L., Guo, L., 2013. Phenolic glucosides from *Dendrobium aurantiacum* var. *denneanum* and their bioactivities. *Molecules* 18, 6153–6160. <https://doi.org/10.3390/molecules18066153>.
- Xiong, L., Zhou, Q.M., Peng, C., Xie, X.F., Liu, L.S., Guo, L., He, Y.C., Yang, L., Liu, Z.H., 2015a. Bis-spirolabdane diterpenoids from *Leonurus japonicus* and their anti-platelet aggregative activity. *Fitoterapia* 100, 1–6. <https://doi.org/10.1016/j.fitote.2014.11.003>.
- Xiong, L., Zhou, Q.M., Zou, Y., Chen, M.H., Guo, L., Hu, G.Y., Liu, Z.H., Peng, C., 2015b. Leonotuketal, a spiroketal diterpenoid from *Leonurus japonicus*. *Org. Lett.* 17, 6238–6241. <https://doi.org/10.1021/acs.orglett.5b03227>.
- Ye, M., Xiong, J., Zhu, J.J., Hong, J.L., Zhao, Y., Fan, H., Yang, G.X., Xia, G., Hu, J.F., 2014. Leonurosolanolides E–J, minor spirocyclic triterpenoids from *Leonurus japonicus* fruits. *J. Nat. Prod.* 77, 178–182. <https://doi.org/10.1021/np400838a>.
- Yin, X., Lu, Y., Cheng, Z.H., Chen, D.F., 2016. Anti-complementary components of *Helicteres angustifolia*. *Molecules* 21, 1–9. <https://doi.org/10.3390/molecules21111506>.
- Zhao, M.Z., Shen, Y., Xu, W., Chen, Y.Z., Xiao, C.J., Jiang, B., 2020. A new lignan glycoside from *Astragalus yunnanensis*. *J. Asian Nat. Prod. Res.* 22, 594–600. <https://doi.org/10.1080/10286020.2019.1607840>.
- Zhou, F., Liu, F., Liu, J., He, Y.L., Zhou, Q.M., Guo, L., Peng, C., Xiong, L., 2020. Stachydrine promotes angiogenesis by regulating the VEGFR2/MEK/ERK and mitochondrial-mediated apoptosis signaling pathways in human umbilical vein endothelial cells. *Biomed. Pharmacother.* 131, 110724. <https://doi.org/10.1016/j.biopha.2020.110724>.
- Zhou, Q.M., Peng, C., Li, X.H., Xiong, L., He, C.J., Guo, L., Cao, Z.X., Liu, Z.H., 2013. Aromatic compounds from *Leonurus japonicus* Houtt. *Biochem. Syst. Ecol.* 51, 101–103. <https://doi.org/10.1016/j.bse.2013.08.023>.
- Zhou, Q.M., Peng, C., Yang, H., Liu, L.S., Yang, Y.T., Xie, X.F., Guo, L., Liu, Z.H., Xiong, L., 2015. Steroids from the aerial parts of *Leonurus japonicus*. *Phytochem. Lett.* 12, 287–290. <https://doi.org/10.1016/j.phytol.2015.04.027>.
- Zhou, Q.M., Zhu, H., Peng, R., Peng, C., Yang, H., Liu, F., Wang, Y.N., Xiong, L., 2019. New triterpenoids from *Leonurus japonicus* (Lamiaceae). *Biochem. Syst. Ecol.* 82, 27–30. <https://doi.org/10.1016/j.bse.2018.11.003>.
- Zhuang, P.Y., Chen, M.H., Wang, Y.N., Wang, X.X., Feng, Y.J., Zhang, D., Yang, 2018. Neolignan and phenylpropanoid compounds from the fruits of *Illicium simonsii* Maxim. *Nat. Prod. Res.* 32, 2468–2475. <https://doi.org/10.1080/14786419.2017.1422179>.
- Zou, Y.H., Zhao, L., Xu, Y.K., Bao, J.M., Liu, X., Zhang, J.S., Li, W., Ahmed, A., Yin, S., Tang, G.H., 2018. Anti-inflammatory sesquiterpenoids from the Traditional Chinese Medicine *Salvia plebeia*: regulates pro-inflammatory mediators through inhibition of NF-κB and Erk1/2 signaling pathways in LPS-induced Raw264.7 cells. *J. Ethnopharmacol.* 210, 95–106. <https://doi.org/10.1016/j.jep.2017.08.034>.
- Zuo, J., Zhang, T.H., Peng, C., Xu, B.J., Dai, O., Lu, Y., Zhou, Q.M., Xiong, L., 2024. Essential oil from *Ligusticum chuanxiong* Hort. alleviates lipopolysaccharide-induced neuroinflammation: Integrating network pharmacology and molecular mechanism evaluation. *J. Ethnopharmacol.* 319, 117337. <https://doi.org/10.1016/j.jep.2023.117337>.